

# hiPSC-derived *GRN*-deficient astrocytes delay spiking activity of developing neurons

Christopher Lee<sup>a,b</sup>, Jonathan Frew<sup>a,b</sup>, Nicholas L. Weilingner<sup>a,c</sup>, Stefan Wendt<sup>a,c</sup>, Wenji Cai<sup>a,b</sup>, Stefano Sorrentino<sup>a,b</sup>, Xiujuan Wu<sup>a,b</sup>, Brian A. MacVicar<sup>a,c</sup>, Stephanie M. Willerth<sup>a,d</sup>, Haakon B. Nygaard<sup>a,b,\*</sup>

<sup>a</sup> Djavad Mowafaghian Centre for Brain Health, University of British Columbia, Vancouver, Canada

<sup>b</sup> Division of Neurology, University of British Columbia, Vancouver, Canada

<sup>c</sup> Department of Psychiatry, University of British Columbia, Vancouver, Canada

<sup>d</sup> Department of Mechanical Engineering and Division of Medical Sciences, University of Victoria, Victoria, Canada

## ARTICLE INFO

### Keywords:

Frontotemporal dementia  
Progranulin  
hiPSC  
Astrocytes  
Neurons  
Multielectrode array  
Neuronal spiking

## ABSTRACT

Frontotemporal dementia (FTD) refers to a group of neurodegenerative disorders that are characterized by pathology predominantly localized to the frontal and temporal lobes. Approximately 40% of FTD cases are familial, and up to 20% of these are caused by heterozygous loss of function mutations in the gene encoding for progranulin (PGRN), *GRN*. The mechanisms by which loss of PGRN leads to FTD remain incompletely understood. While astrocytes and microglia have long been linked to the neuropathology of FTD due to mutations in *GRN* (FTD-*GRN*), a primary mechanistic role of these supporting cells have not been thoroughly addressed. In contrast, mutations in *MAPT*, another leading cause of familial FTD, greatly alters astrocyte gene expression leading to subsequent non-cell autonomous effects on neurons, suggesting similar mechanisms may be present in FTD-*GRN*. Here, we utilized human induced pluripotent stem cell (hiPSC)-derived neural tissue carrying a homozygous *GRN* R493X<sup>-/-</sup> knock-in mutation to investigate in vitro whether *GRN* mutant astrocytes have a non-cell autonomous effect on neurons. Using microelectrode array (MEA) analysis, we demonstrate that the development of spiking activity of neurons cultured with *GRN* R493X<sup>-/-</sup> astrocytes was significantly delayed compared to cultures with WT astrocytes. Histological analysis of synaptic markers in these cultures showed an increase in GABAergic synaptic markers and a decrease in glutamatergic synaptic markers during this period when activity was delayed. We also demonstrate that this effect may be due in-part to soluble factors. Overall, this work represents one of the first studies investigating astrocyte-induced neuronal pathology in *GRN* mutant hiPSCs, and supports the hypothesis of astrocyte involvement in the early pathophysiology of FTD.

## 1. Introduction

Frontotemporal dementia (FTD) represents a set of devastating neurodegenerative syndromes leading to progressive loss of behavioral control, executive function, memory and language (Bott et al., 2014). On average, FTD accounts for 10% of dementia cases younger than 65 years of age, and approximately 3% of all dementia cases, although this is likely an underestimate given diagnostic challenges in this population (Hogan et al., 2016). Approximately 40% of FTD patients show a familial inheritance pattern, with 10% displaying autosomal dominant inheritance (Rabinovici and Miller, 2010). *GRN*, encoding the highly conserved secreted protein progranulin (PGRN), is a commonly mutated

gene in familial FTD, accounting for 5–20% of cases (Cruts et al., 2006; Olszewska et al., 2016; Baker et al., 2006). The mechanisms by which *GRN* haploinsufficiency leads to neurodegeneration are not fully understood, but accumulating evidence suggests multifaceted pathophysiology including lysosomal dysfunction, neuroinflammation, and profound synaptic dysfunction (Nicholson et al., 2012; Mackenzie, 2007). In mice lacking *GRN*, synaptic dysfunction appears to precede microgliosis and lipofuscinosis, suggesting a more direct impact of PGRN on synaptic pathology prior to well characterized FTD-*GRN* neuropathology (Petkau et al., 2012). Corroborating these findings, *GRN* insufficiency leads to reduced connectivity and synapse density in rat hippocampal neurons, and multiple lines of evidence, including

\* Corresponding author at: Djavad Mowafaghian Centre for Brain Health, University of British Columbia, Vancouver, British Columbia V6T 1Z3, Canada.

E-mail address: [haakon.nygaard@ubc.ca](mailto:haakon.nygaard@ubc.ca) (H.B. Nygaard).

<https://doi.org/10.1016/j.nbd.2023.106124>

Received 3 November 2021; Received in revised form 3 March 2023; Accepted 10 April 2023

Available online 11 April 2023

0969-9961/© 2023 The Authors. Published by Elsevier Inc. This is an open access article under the CC BY license (<http://creativecommons.org/licenses/by/4.0/>).

proteomic and transcriptomic profiles, implicate synaptic dysfunction in a cellular *GRN*<sup>-/-</sup> model (Chitramuthu et al., 2021; Tapia et al., 2011).

Most in vitro studies of PRGN function to date have investigated isolated neuronal pathophysiology, without considering contributions from supporting cells that are vital for synaptic health. Indeed, despite the critical role of astrocytes in the genesis, maturation, modulation, and maintenance of neurons and the neural network (Hedegaard et al., 2020), their direct role in FTD-GRN has only very recently been suggested as *GRN* null astrocytes were found sufficient to cause TAR-DNA binding protein 43 (TDP-43) deposits in a 3D iPSC organoid structure (de Majo et al., 2023). A 2017 study by Hallmann et al. reported that human induced pluripotent stem cell (hiPSC)-derived astrocytes carrying the N279K FTD-causing mutation in *MAPT* showed non-cell autonomous effects on co-cultured neurons (Hallmann et al., 2017). Specifically, it was found that astrocytes themselves displayed altered global expression in genes related to synapse organization, stress-response, and multicellular organism development. Neurons co-cultured with *MAPT* mutant astrocytes displayed dysfunction in their oxidative stress response, and altered gene expression in genes related to regulation of cellular and system processes, stress, and apoptosis (Hallmann et al., 2017). These results imply a possible functional role for astrocytes in FTD, specifically one that can be elucidated by the use of hiPSC-derived astrocytes harboring FTD-causing mutations. Contrary to previous work, (Petkau et al., 2010), more recent evidence from a number of human and mouse studies has measured significant astrocyte secretion of PGRN (Zhang et al., 2020; Suh et al., 2012; Frew et al., 2020; Götzl et al., 2018), indicating an active role of astrocyte in PGRN-mediated cellular functions. The major objective of the present study was to investigate the effects of *GRN* mutant astrocytes on in vitro development of electrical activity in differentiated neurons in a hiPSC model of *GRN* deficiency.

## 2. Methods and materials

### 2.1. hiPSC culture

The work on hiPSCs reported here was approved by the University of British Columbia Clinical Research Ethics Board (H21-02261). The two lines of hiPSC cells used in this study were i) hiPSC line reprogrammed from peripheral blood obtained from a healthy control subject (WT) and ii) an isogenic hiPSC line homozygous for *GRN* R493X knock-in (*R493X*<sup>-/-</sup>) produced from the WT line as previously described (Frew et al., 2020). hiPSC lines were assessed for expression of pluripotent markers at the protein and mRNA level, their ability to differentiate into all three germ layers, and demonstrated that they were all karyotypically normal at passage 11 for WT cell lines and passage 27 for *R493X*<sup>-/-</sup> cell lines (Frew et al., 2020). The current experiments used hiPSCs at passage 11–15 for WT cells and 27–29 for *R493X*<sup>-/-</sup> cells. Mycoplasma testing was last performed at P14 for WT cells and P29 for *R493X*<sup>-/-</sup> hiPSCs using the MycoProbe® Mycoplasma Detection Kit (R&D Systems, Minneapolis, USA).

Cells were maintained on 6-well Matrigel (BD Biosciences, Franklin Lakes, USA) coated plates in mTeSR1 medium (STEMCELL Technologies, Vancouver, Canada). Media was changed daily or after 48 h if given double media. After cells reached 80% confluence, cells were passaged as aggregates using ReLeSR (STEMCELL Technologies) at a 1:3 ratio. Cells were plated onto a new, 6-well, Matrigel coated plate in mTeSR1 supplemented with 10  $\mu$ M of the rho-associated protein kinase inhibitor Y-27632 (EMD Millipore, Burlington, USA). Media was changed after 24 h to mTeSR1 without Y-27632 supplementation, and culture continued as previously described (Frew et al., 2020). Cells were frozen into liquid nitrogen (LN) as needed in mTeSR1 + 10  $\mu$ M Y-26732 + 10% DMSO (Millipore Sigma, Burlington, USA).

### 2.2. Neural lineage differentiation

WT and *R493X*<sup>-/-</sup> hiPSCs were differentiated into NPCs using a 23-day dual SMAD inhibition protocol as previously described, yielding >95% neuron purity by MAP2/GFAP staining (Frew et al., 2020; Rose et al., 2018). A portion of these NPCs were frozen into LN for future use in Neural Stem Cell (NSC) media. NPCs were then differentiated into astrocytes utilizing the STEMdiff™ Astrocyte Differentiation Kit and STEMdiff™ Astrocyte Maturation Kit™ (STEMCELL Technologies) according to the manufacturer's 35-day protocol with Matrigel-coated plates. Expansion of astrocytes was performed by continuing to change media every 2–3 days with the Astrocyte Maturation Kit™ and passaging the cells at 90% confluence using Accutase (EDM Millipore) at a 1:3 ratio onto Matrigel-coated plates. Cells were frozen into LN as needed in Astrocyte Maturation Media +10% DMSO.

### 2.3. Mixed MEA culture

Previously frozen NPCs were thawed onto Matrigel-coated plates in NSC medium and expanded over 7 days. NPCs and astrocytes were Accutase passaged and mixed 1:1 in the following conditions: i) WT NPCs with WT astrocytes, ii) WT NPCs with *R493X*<sup>-/-</sup> astrocytes, iii) *R493X*<sup>-/-</sup> NPCs with WT astrocytes, and iv) *R493X*<sup>-/-</sup> NPCs with *R493X*<sup>-/-</sup> astrocytes.  $6.0 \times 10^4$  cells/well were suspended in complete BrainPhys™ (STEMCELL Technologies) media system (Bardy et al., 2015) supplemented with 1 $\times$  CultureOne™ (Gibco, Thermo Fisher Scientific, Waltham, USA) and 10% Matrigel, then plated onto a poly-L-ornithine (Millipore Sigma) and laminin (Millipore Sigma) (PLO/Lam) coated 48-well CytoView MEA plate (Axion Biosystems, Atlanta, USA) with only enough media to cover the electrode. The NPC/astrocyte mixes were then incubated for 45 min at tissue culture conditions to allow for adhesion to the electrode before further media was added. NPCs were then differentiated into neurons according to our previously described BrainPhys™ protocol (Frew et al., 2020), and MEA recordings were taken daily with aa MaestroPro MEA plate reader (Axion Biosystems, Atlanta, USA). Wells that failed to survive were excluded from the analysis.  $n = 3$  separate NPC to neuron differentiations per condition were pooled in the analysis, with total wells equalling  $n = 39$  WT NPCs with WT astrocytes,  $n = 41$  WT NPCs with *R493X*<sup>-/-</sup> astrocytes,  $n = 33$  *R493X*<sup>-/-</sup> NPCs with WT astrocytes, and  $n = 29$  *R493X*<sup>-/-</sup> NPCs with *R493X*<sup>-/-</sup> astrocytes.

### 2.4. Insert MEA culture

Previously frozen NPCs were thawed onto Matrigel-coated plates in NSC medium and expanded over 7 days.  $3.0 \times 10^4$ /well WT and  $3.0 \times 10^4$ /well *R493X*<sup>-/-</sup> NPCs were suspended in complete BrainPhys™ media system supplemented with 1 $\times$  CultureOne™ and 10% Matrigel, then plated onto a PLO/Lam coated 24-well CytoView MEA plates. Separately, WT and *R493X*<sup>-/-</sup> astrocytes were plated onto Matrigel-coated, 12 mm, polycarbonate, 0.4  $\mu$ m cell culture insert (Millipore Sigma) at  $6.0 \times 10^4$  cells per insert and allowed to attach overnight. The following day (Day 1 of MEA culture) the astrocyte insert was added to the MEA plate and NPCs were differentiated into neurons as described above. MEA recordings were taken every 2–4 days with a MaestroPro MEA plate reader (Axion Biosystems, Atlanta, USA). Wells that failed to survive or dysfunctional electrodes were excluded from the analysis.  $n = 4$  separate NPC to neuron differentiations per condition were pooled in the analysis, with total wells equalling  $n = 24$  WT NPCs with WT astrocytes,  $n = 22$  WT NPCs with *R493X*<sup>-/-</sup> astrocytes,  $n = 21$  *R493X*<sup>-/-</sup> NPCs with WT astrocytes, and  $n = 24$  *R493X*<sup>-/-</sup> NPCs with *R493X*<sup>-/-</sup> astrocytes.

### 2.5. MEA data acquisition and analysis

MEA plates were recorded using a MaestroPro MEA plate reader

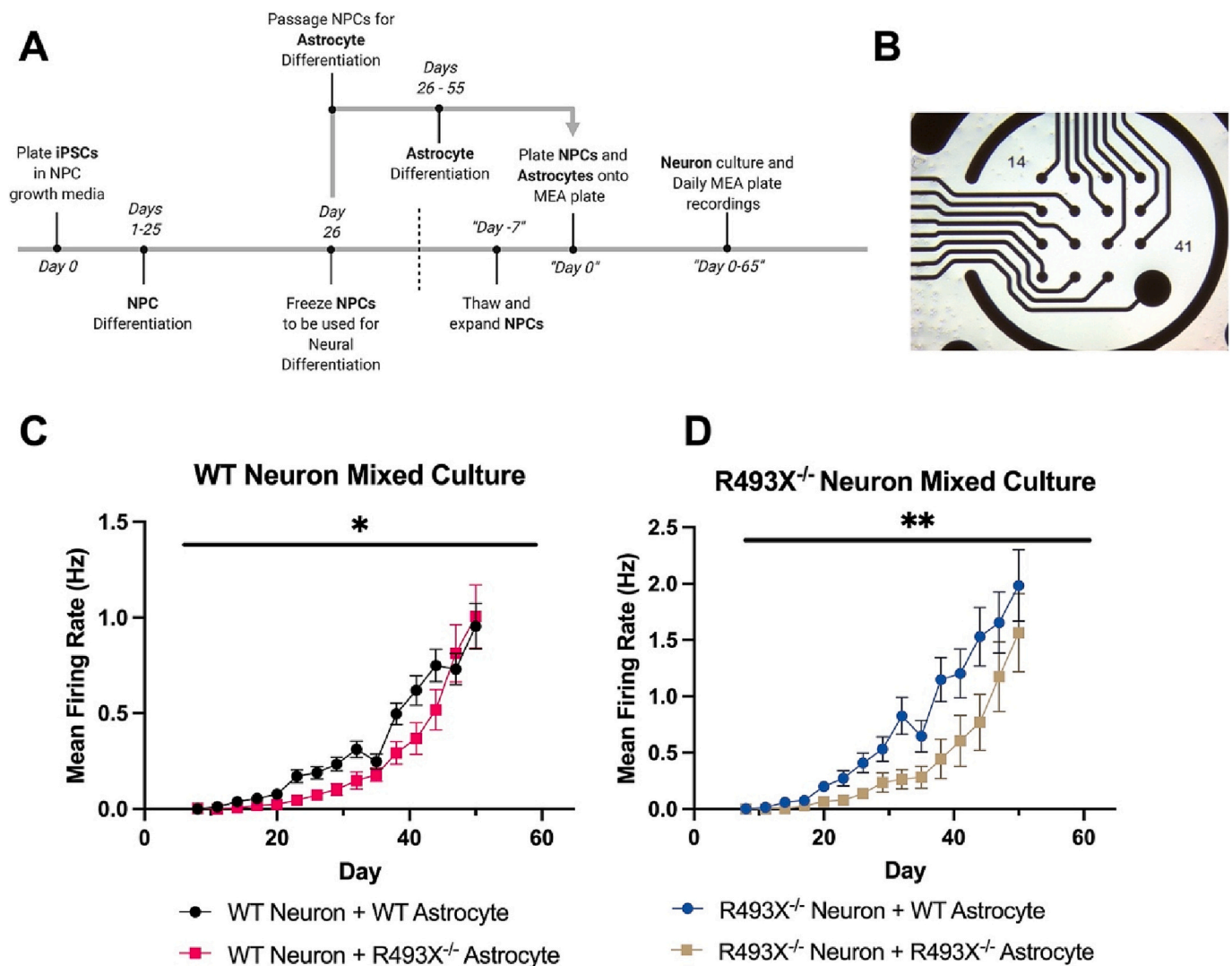


**Fig. 1.** *GRN* R493X<sup>-/-</sup> FTD astrocytes delay spiking activity in developing neurons in neuron/astrocyte co-cultures. hiPSC neurons and astrocytes from a healthy non-demented individual (WT) and its *GRN* R493X knock-in CRISPR-edited isogenic clone (R493X<sup>-/-</sup>) were differentiated into astrocytes and neurons (A) and then plated together on an MEA plate (B). Cells were mixed in four conditions i) WT neurons with WT astrocytes, ii) WT neurons with R493X<sup>-/-</sup> astrocytes, iii) R493X<sup>-/-</sup> neurons with WT astrocytes, and iv) R493X<sup>-/-</sup> neurons with R493X<sup>-/-</sup> astrocytes. Compared to WT astrocytes, R493X<sup>-/-</sup> astrocytes delayed development of excitatory electrical signaling in both WT neurons (C) and R493X<sup>-/-</sup> neurons (D), with the latter being slightly more pronounced. Values represent the mean of the average of 3 biological replicates  $\pm$  SEM. \* $p$  < 0.05, \*\* $p$  < 0.01, by two-way RM ANOVA.

running the AxIS Navigator 3.4.1 software (Axion Biosystems Inc., Atlanta, USA). Legitimacy of cell activity was assessed using the Continuous Waveform Plots function of the AxIS Navigator. Spontaneous activity from raw MEA data files were converted to .CSV files in AxIS Navigator, and files from a single plate were compiled and plotted using the AxIS Metric Plotting Tool. Data was exported using the "Recommended Metrics" function. Activity of cells was assessed using the Mean Firing Rate – which is a measure of all instances of electrical activity, or spikes, detected by the MEA. Percent active wells was assessed using the Active Electrodes metric – which is a measure of electrodes determined to be significantly active by the AxIS Navigator software. Wells with  $\geq 1$  active electrode were considered active.

## 2.6. Immunocytochemistry imaging

Previously frozen NPCs were thawed onto Matrigel-coated plates in NSC medium and expanded over 7 days. 24-well plates containing glass coverslips were coated with PLO/Lam and then plated with WT and R493X<sup>-/-</sup> NPCs and astrocytes in the same four conditions and

differentiated as described above. To prepare coverslip cultures for imaging, cells were fixed with 4% paraformaldehyde (ThermoFisher Scientific) for 15 min and washed three times with PBS (ThermoFisher Scientific). Cells were blocked and permeabilized with 10% donkey, 10% goat serum (Millipore Sigma) in PBS containing 0.1% Triton X-100 (Abcam) for 1 h at room temperature (RT). Anti-beta-tubulin III (TUJ1) monoclonal chicken (Neuromics: Catalog#CH23005), anti-vesicular glutamate transporter 1 (vGLUT1) monoclonal mouse (Synaptic Systems: Catalog#135311), anti-glutamic acid decarboxylase 65/67 (GAD) polyclonal rabbit (Millipore Sigma: Catalog#G5163), and anti-gial fibrillary acidic protein (GFAP) polyclonal primary polyclonal rabbit (STEMCELL: Catalog# 60128) antibodies were diluted 1:500, 1:200, 1:500, and 1:500 respectively, in 10% donkey, 10% goat serum in PBS and applied to cells overnight at 4 °C. Alexa Fluor®-tagged secondary antibodies goat anti-chicken 488 (ThermoFisher Scientific), donkey anti-mouse 568 (ThermoFisher Scientific), donkey anti-rabbit 647 (ThermoFisher Scientific) were applied at a dilution of 1:500 at RT for 2 h. Coverslips were then mounted in DAPI mounting medium (Vector Laboratories) onto a glass slide and imaged using a Zeiss 880 scanning



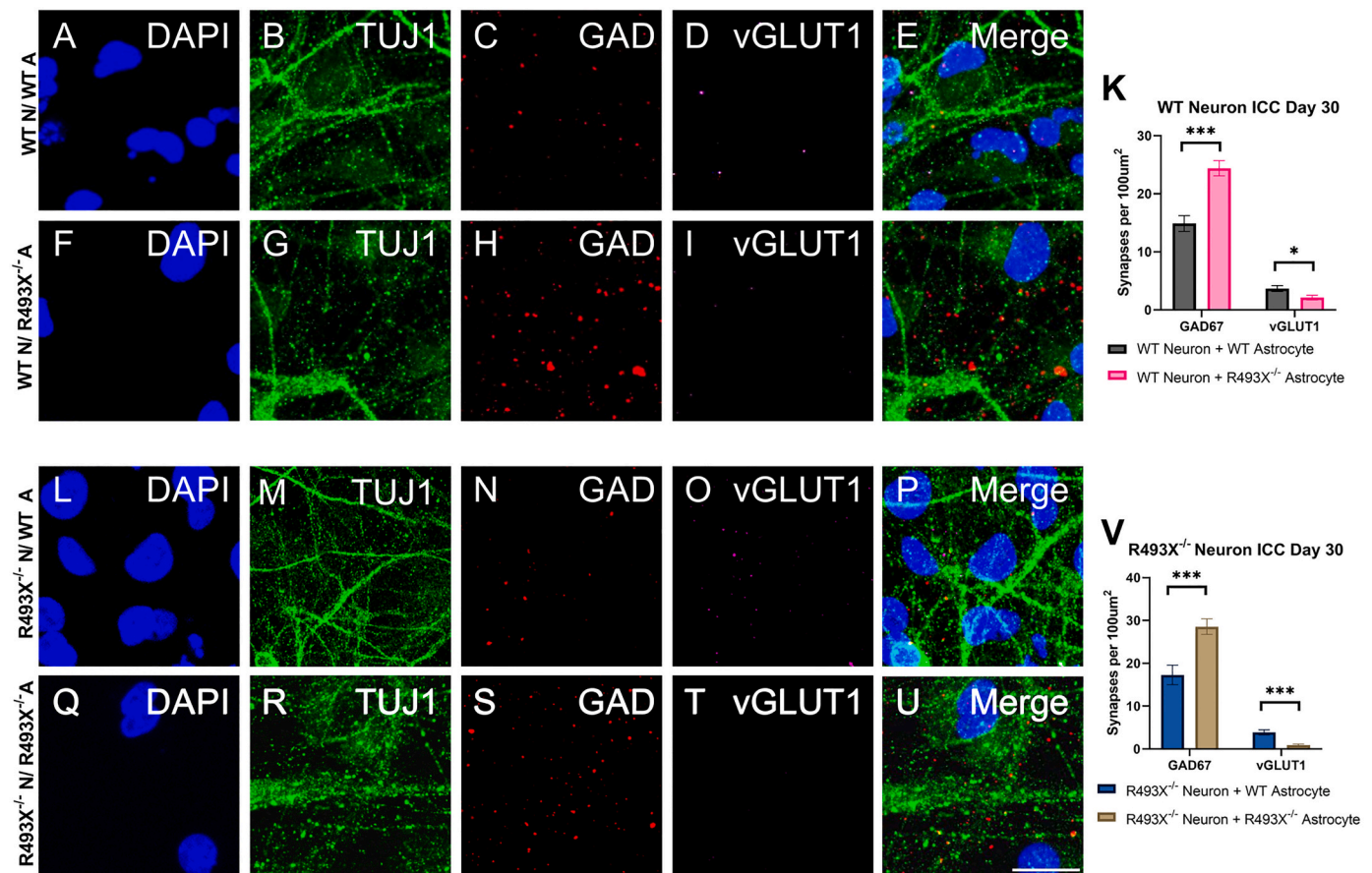


**Fig. 2.** *GRN* R493X<sup>-/-</sup> FTD astrocytes impair vGLUT1 glutamatergic synapse formation and facilitates GABAergic synapse formation in Day 30 neurons. Day 30 and WT and R493X<sup>-/-</sup> neuron/astrocyte co-cultures were stained for DAPI, TUJ1, GAD, and vGLUT1, and imaged using ICC and confocal microscopy (A–J, L–U). Glutamatergic and GABAergic synapses were measured by counting the number of individual synapses in FIJI (ImageJ) and then standardizing the number with neuron area estimated with the TUJ1 stain (K, V). Scale bar represents 20 μm. Values represented as mean ± SEM, 3 random fields each from triplicate replicates of *N* = 3 independent NPC differentiations resulted in a total of 36 fields per condition, \**P* < 0.05, \*\*\**P* < 0.001 by two-tailed Student's *t*-test.

laser confocal microscope running ZEN 2 software. For synaptic quantification, image analysis was performed using FIJI and uniform threshold options for all images of the same primary antibody and NPC differentiation. Number of synapses was quantified by measuring the number of unique vGLUT1 and GAD puncta determined via FIJI particle analysis and standardizing it to neuronal area estimated as TUJ1 area as previously described (Frew et al., 2020). *n* = 3 NPC to neuron differentiations per condition was used for this analysis with *n* = 3 unique slides. *n* = 3 random fields of view were used per slide. For astrocyte quantification, percent astrocytes was determined by manually counting the number of GFAP+ cells and dividing by the total number of DAPI+ nuclei determined by applying uniform thresholds and converting images to binary using the watershed segmentation tool and quantifying the number of individual DAPI+ cells with the analyze particles function. *n* = 1 NPC to neuron differentiation per condition was used for this analysis with *n* = 3 unique slides. *n* = 3 random fields of view were used per slide.

## 2.7. Data visualization and statistical analysis

All graphing and statistical analysis were performed using the GraphPad Prism 9 software. Data points in all figures represent the mean of the average of 3 biological replicates, and statistical analysis was performed on this data. A biological replicate was defined as an independent NPC to neuron/astrocyte differentiation. Results are reported as mean ± standard error of the mean (SEM). Comparisons between two groups was performed done using a standard unpaired two-tailed

Student's *t*-test, and reported as a *p*-value following results. Comparisons between two or more groups with multiple time points was done using a repeated measures two-way analysis of variance (RM Two-Way ANOVA) followed by Bonferroni post hoc analysis comparing means of individual time points for MEA results, comparing means of individual time points, and comparing between time points of individual culture conditions for percent astrocyte ICC results. RM Two-Way ANOVA significance was reported as the factor investigated (time x astrocyte interaction) *P*-value, *F*, and degrees of freedom (DoF). Time to active MEA wells was analyzed using the logrank test (Mantel-Cox). Statistical significance was defined as minimum *P* < 0.05.

## 3. Results

### 3.1. Loss of *PGRN* delays neuronal synaptic maturation in an astrocyte-dependent manner

An hiPSC line acquired from a healthy non-demented individual (WT) and its *GRN* R493X knock-in CRISPR-edited isogenic clone (R493X<sup>-/-</sup>) were differentiated into NPCs, and a portion of the NPCs were further differentiated into cortical astrocytes (Fig. 1A). NPCs were plated together on an MEA plate (Fig. 1B) with astrocytes in four separate mixes i) WT NPCs with WT astrocytes, ii) WT NPCs with R493X<sup>-/-</sup> astrocytes, iii) R493X<sup>-/-</sup> NPCs with WT astrocytes, and iv) R493X<sup>-/-</sup> NPCs with R493X<sup>-/-</sup> astrocytes. NPCs were differentiated into neurons and electrical recordings were taken daily over 50 days on an Axion Biosystems MEA plate and reader, which evaluates

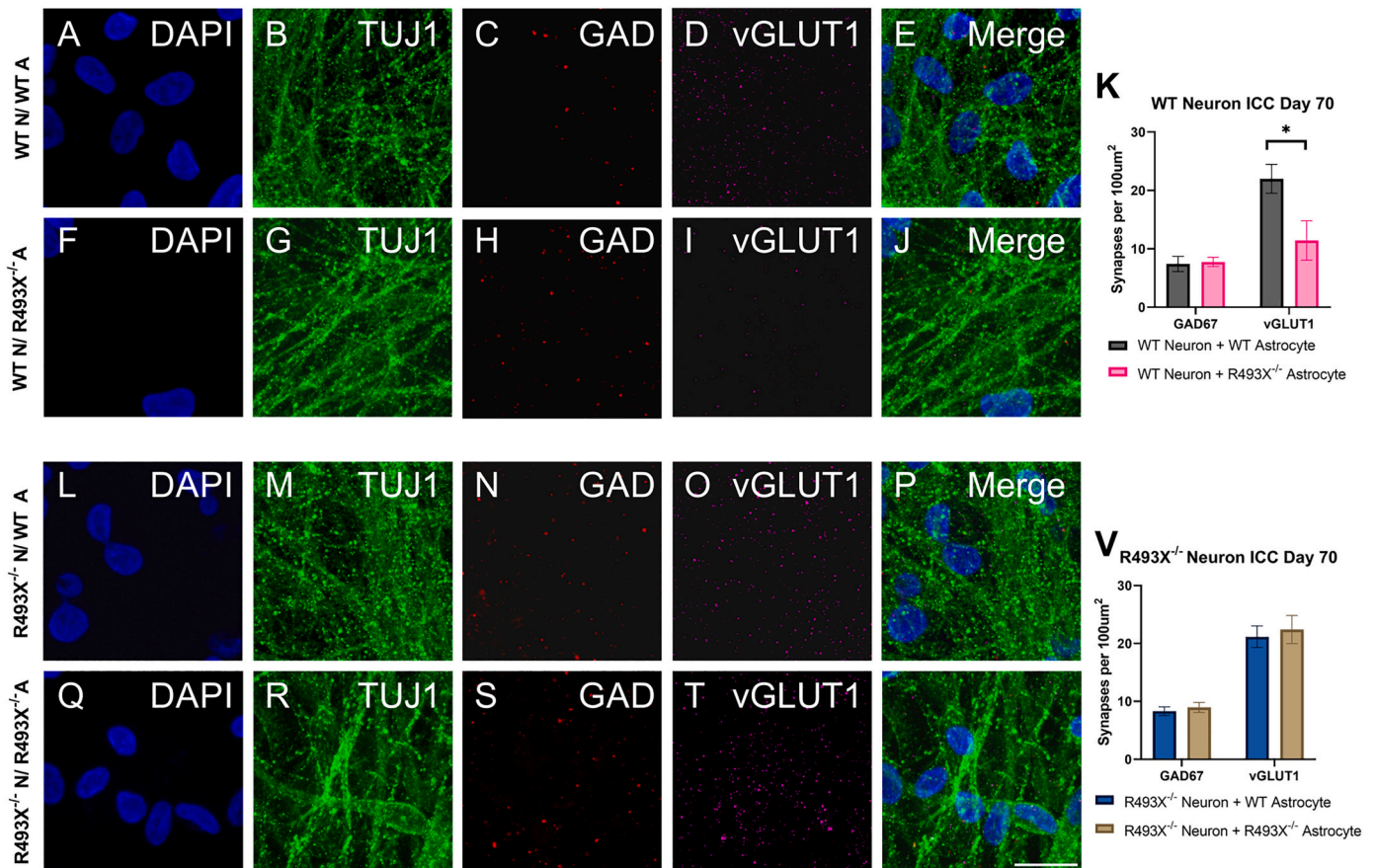


**Fig. 3.** GRN R493X<sup>-/-</sup> astrocyte condition neurons show partial recovery of normal vGLUT1 glutamatergic and GAD GABAergic synapse levels. Day 70 and WT and R493X<sup>-/-</sup> neuron/astrocyte co-cultures were stained for DAPI, TUJ1, GAD, and vGLUT1, and imaged using ICC and confocal microscopy (A–J, L–U). Glutamatergic and GABAergic synapses were measured by counting the number of individual synapses in FIJI and then standardizing the number with neuron area estimated with the TUJ1 stain (K, V). Scale bar represents 20 μm. Values represented as mean ± SEM, 3 random fields from triplicate replicates of N = 3 independent NPC differentiations resulted in a total of 36 fields per condition, \*P < 0.05 by two-tailed Student's t-test.

longitudinal electrical activity via measurement of spontaneous electrical spiking. For both WT and R493X<sup>-/-</sup> neuron cultures, development of excitatory electrical activity as inferred from mean firing rate was significantly delayed when neurons were differentiated in the presence of R493X<sup>-/-</sup> astrocytes compared to WT astrocytes (Fig. 1C, D). Combining WT neurons with R493X<sup>-/-</sup> astrocytes lead to a significant delay in spiking activity compared to WT neurons with WT astrocytes (time x astrocyte interaction,  $P = 0.0392$ ,  $F = 1.764$ ,  $\text{DoF} = 14$ ) (Fig. 1C). Similarly, cultured R493X<sup>-/-</sup> neurons with R493X<sup>-/-</sup> astrocytes lead to an even more significant delay in spiking activity compared to R493X<sup>-/-</sup> neurons with WT astrocytes (time x astrocyte interaction,  $P = 0.0076$ ,  $F = 2.168$ ,  $\text{DoF} = 14$ ) (Fig. 1D). In cultures with R493X<sup>-/-</sup> astrocytes, spiking activity eventually caught up with WT astrocyte cultures by day 50 (Fig. 1C, D).

### 3.2. GRN R493X<sup>-/-</sup> FTD astrocytes impair vGLUT1 glutamatergic synapse formation and facilitates GABAergic synapse formation

In order to quantify synaptic changes underlying electrophysiological changes, we performed immunocytochemistry (ICC) and confocal microscopy to quantify presence of excitatory and inhibitory synapses in our neuron/astrocyte co-cultures. We performed imaging on cultures aged 30 and 70 days for the mixes of i) WT neurons with WT astrocytes (Fig. 2A–E, Fig. 3A–E), ii) WT neurons with R493X<sup>-/-</sup> astrocytes (Fig. 2F–J, Fig. 3F–J), iii) R493X<sup>-/-</sup> neurons with WT astrocytes (Fig. 2L–P, Fig. 3L–P), and iv) R493X<sup>-/-</sup> neurons with R493X<sup>-/-</sup> astrocytes (Fig. 2Q–U, Fig. 3Q–U). For the WT neuron conditions, we observed a

statistically significant decrease in the number of vGLUT1 synapses per 100 mm<sup>2</sup> when WT neurons were cultured with R493X<sup>-/-</sup> astrocytes ( $2.13 \pm 0.42$ ) when compared to WT astrocytes ( $3.70 \pm 0.51$ ) at day 30 ( $P = 0.02$ ) (Fig. 2K). WT neurons with R493X<sup>-/-</sup> astrocytes also showed a significant increase in GABAergic synapses ( $24.39 \pm 1.32$ ) compared to WT neurons with WT astrocytes ( $14.88 \pm 1.35$ ) ( $P < 0.001$ ) (Fig. 2K).

For the second timepoint of day 70 (Fig. 3K), the number of GABAergic synapses decreased from day 30 and was not significantly different when comparing both the WT astrocyte ( $9.48 \pm 1.54$ ) and the R493X<sup>-/-</sup> astrocyte ( $9.03 \pm 0.89$ ) conditions ( $P = 0.80$ ). Conversely, the number of glutamatergic synapses on day 70 was considerably higher than day 30 for both astrocyte conditions, and the WT astrocyte condition ( $26.11 \pm 2.83$ ) was significantly higher than its R493X<sup>-/-</sup> counterpart ( $13.21 \pm 4.46$ ) ( $P = 0.018$ ), indicating some persistent excitatory-inhibitory imbalance at this timepoint despite normalized MEA signal.

For the R493X<sup>-/-</sup> neurons, we again observed a statistically significant day 30 decrease in glutamatergic synapses in the R493X<sup>-/-</sup> astrocyte condition ( $0.92 \pm 0.24$ ) compared to the WT astrocyte condition ( $3.89 \pm 0.59$ ) ( $P < 0.001$ ) (Fig. 2V). The R493X<sup>-/-</sup> astrocyte condition also significantly increased the number of GABAergic synapses ( $28.56 \pm 1.81$ ) compared to the WT astrocyte condition ( $17.30 \pm 2.27$ ) ( $P < 0.001$ ) (Fig. 2V). At day 70 the changes observed at day 30 had largely resolved, with no significant difference observed between the WT and R493X<sup>-/-</sup> astrocyte conditions for either the glutamatergic synapses ( $24.34 \pm 2.09$  for the WT astrocytes and  $26.38 \pm 2.82$  for the R493X<sup>-/-</sup> astrocytes;  $P = 0.56$ ) or the GABAergic synapses ( $8.26 \pm 0.94$

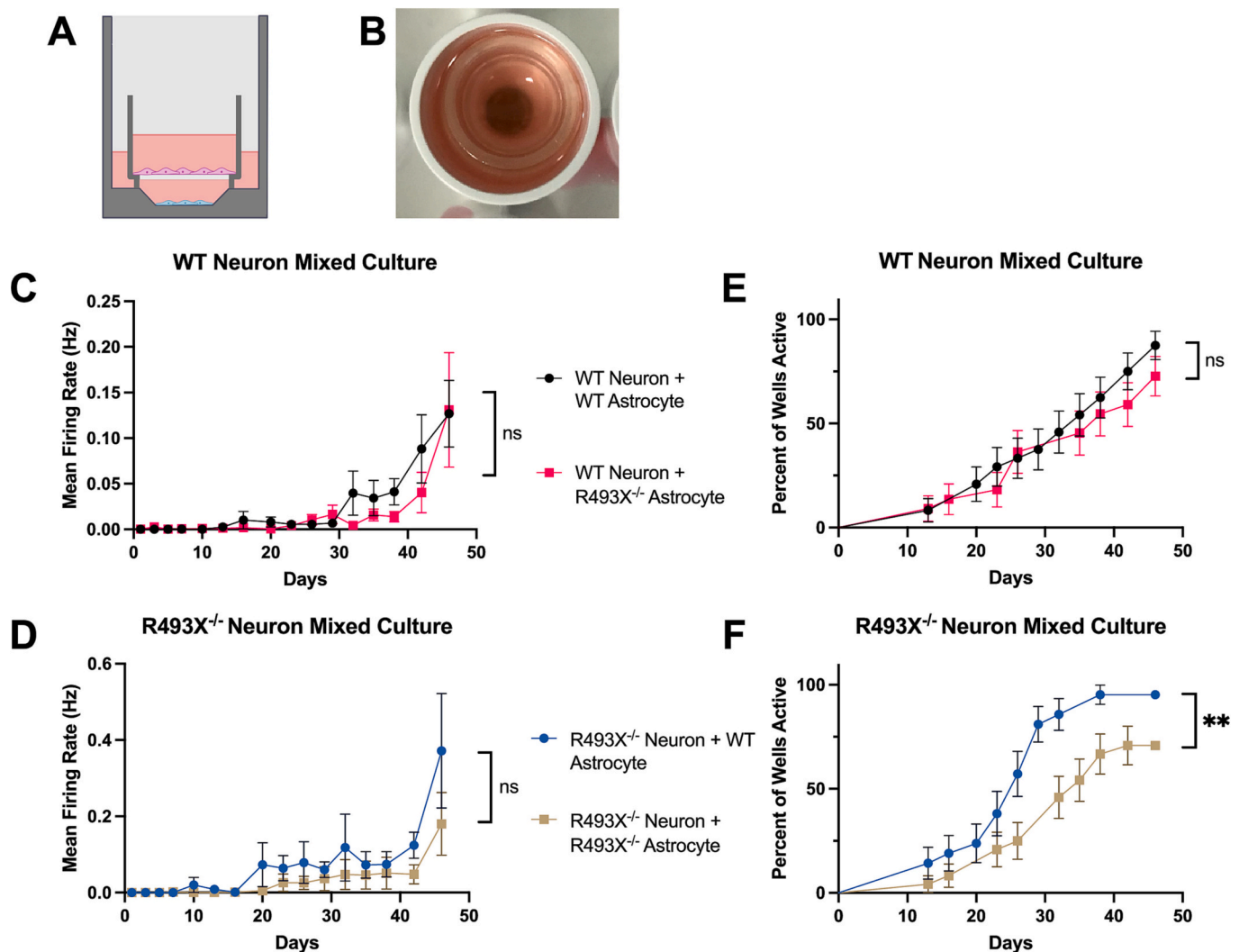


**Fig. 4.** GRN R493X<sup>-/-</sup> FTD astrocytes delay electrical development partially due to a soluble factor. Astrocytes plated on cell culture inserts were used to separate astrocytes from neurons and evaluate contribution from soluble factors: (A) Diagram of the inserts used and (B) image of the insert within a well. Separated neurons were measured every 2–4 days for 46 days on an MEA plate for (C) WT neuron mixes and (D) R493X<sup>-/-</sup> neuron mixes. Percent active wells was assessed using the Active Electrodes metric and represented as a percent of total wells for (E) WT neuron mixes and (F) R493X<sup>-/-</sup> neuron mixes. Omitted data points in panels E,F represent timepoints with no change in number of active electrodes. Values represented as mean  $\pm$  SEM. \*\* $P = 0.0019$  by the logrank (Mantel-Cox) test.

for the WT astrocytes and  $9.98 \pm 0.92$  for the R493X<sup>-/-</sup> astrocytes;  $P = 0.20$ ).

Taken together, the histologic findings largely mirror results from the MEA, with R493X<sup>-/-</sup> astrocytes mediating decreased glutamatergic signaling, with a concomitant increase in GABAergic signaling, which resolve, at least partially, by day 70. Additional co-culture staining was performed to determine whether differences in astrocyte numbers was contributing to the observed phenotype. ICC performed at days 1, 30, and 60 using GFAP as a marker for astrocytes and TUJ1 as a marker for neurons revealed a time-dependent decrease in the percent of astrocytes in all conditions, but no difference was found between groups at any timepoint (Fig. S1).

### 3.3. GRN R493X<sup>-/-</sup> FTD astrocytes delay electrical development partially due to a soluble factor

To determine whether soluble factors could be contributing to the observed MEA plate phenotype from Section 3.1, we performed a mixed MEA culture with the same mixes as in Section 3.1, but with neurons plated onto the electrodes and astrocytes plated onto a removable cell culture insert (Fig. 4A, B). Electrical development of cultures was

measured over 46 days. Electrical development was markedly slower and less pronounced in both neuron conditions of the insert cultures when compared to the co-cultures where neurons and astrocytes physically interact. For both the WT and R493X<sup>-/-</sup> neuron conditions, a nonsignificant trend was observed towards a delay in mean firing rate in the R493X<sup>-/-</sup> astrocyte condition (Fig. 4C, D). To better understand the variation between individual wells, we examined how many wells were determined to be active by the Axion Navigation software. Comparison between the WT neuron conditions did not reveal any noticeable trend in the differences between percentage of active wells over time (Fig. 4E). However, examination of the R493X<sup>-/-</sup> neuron conditions showed a delay for the R493X<sup>-/-</sup> astrocytes compared to the WT astrocytes ( $P = 0.0019$ ) which remained unresolved at day 46 (Fig. 4F).

## 4. Discussion

Through longitudinal MEA recordings of hiPSC-derived neuronal networks, we show that loss of progranulin expression delays the maturation of neuronal spiking activity through astrocyte-mediated pathways. Thus, when combining neurons lacking PGRN with healthy astrocytes, network spiking activity is significantly improved. In



contrast, healthy neurons combined with astrocytes lacking PRGN delays network maturation, indicating that the development of neuronal spiking activity is greatly influenced by astrocyte PRGN expression. Interestingly, the early delay in synaptic maturation was normalized by day 50 where excitatory electrical activity was similar in all groups, suggesting a compensatory mechanism not yet defined.

Synaptic dysfunction is a key finding in FTD-GRN, and indeed across neurodegenerative syndromes (Mackenzie, 2007; Lepeta et al., 2016). Autopsy studies have revealed profound, regional synaptic loss in patients with FTD-GRN, and functional imaging indicate significant impairments in the neuronal network prior to clinical symptoms (Mackenzie, 2007; Lee et al., 2019). In GRN null mice, regional synaptic loss is similarly prominent (Frew and Nygaard, 2021), and morphological changes to neurons as well as electrophysiologic abnormalities can precede neuropathological changes (Petkau et al., 2012). Despite these established findings, the mechanisms by which PRGN leads to synaptic dysfunction are not well understood. In this context, our data suggest that lack of PRGN may impair synaptic function at the earliest embryonic stage, and that this impairment is at least partly astrocyte dependent. Given the novelty of our findings, both inciting factors and compensatory mechanisms may be highly relevant in patients with FTD-GRN as the same pattern could persist in the adult brain. Furthermore, developmental changes are known to impact adult CNS function. This is perhaps best exemplified by pruning, the process by which synapses are eliminated to create a more efficient neuronal network in response to environmental demands. Pruning depends on synaptic activity (Sretavan et al., 1988), and is implicated as a maladaptive and pathogenic process in models of both FTD-GRN and AD (Lui et al., 2016; Hong et al., 2016). While speculative, abnormal development of the neuronal network may render certain areas more susceptible to toxic-metabolic insults, and thus predispose these areas to hypoactivity and elimination in the adult brain.

In line with MEA results, neurons cultured in the presence of mutated astrocytes had increased expression of the inhibitory GABAergic synapse marker GAD, and decreased expression of the excitatory glutamatergic synapse marker vGLUT1. Altered excitatory/inhibitory (E/I) balance may drive progression of dementia, and glial cells are known to play a role in this progression (Bi et al., 2020; Henstridge et al., 2019). Increased GABAergic markers are in line with previous results from hiPSCs generated from patients suffering from healthy donor-derived, genetically altered triple *MAPT*-mutant hiPSC line which showed increased GABAergic markers (García-León et al., 2018).

While the experiments using astrocytes on inserts provided evidence for a soluble astrocyte factor mediating a delay in neuronal synaptic development, there are two major caveats: First, perturbed development observed in the R493X<sup>-/-</sup> neuron mixes was much more subtle in the insert cultures than when astrocytes were physically interacting with neurons; Second, the effect of delayed signaling was only observed in R493X<sup>-/-</sup> neuron mixes and not WT neuron mixes. The more subtle effect of development is possibly explained by neurons simply maturing more efficiently when physically interacting with astrocytes.

In conclusion, in this report we demonstrate that astrocytes may play a significant role in the early pathophysiology of FTD-GRN. Future studies, utilizing larger libraries of hiPSCs, including heterozygous models, 3D modeling, and studies in humans will elucidate more precise mechanisms that could lead to new insights for drug development in FTD-GRN.

## Competing interests

HBN has served as a member on advisory boards for Biogen and Hoffmann-La Roche. The authors declare no other financial or non-financial conflicts of interest.

## Author contributions

**Christopher Lee:** Conceptualization, Formal analysis, Investigation, Writing - original draft, manuscript review and editing. **Jonathan Frew:** Conceptualization, manuscript review and editing. **Nicholas L. Weillinger:** Investigation, manuscript review and editing. **Stefan Wendt:** Investigation, manuscript review and editing. **Wenji Cai:** Investigation, manuscript review and editing. **Stefano Sorrentino:** Investigation, manuscript review and editing. **Xiujuan Wu:** Resources, manuscript review and editing. **Brian A. MacVicar:** Project supervision, manuscript review and editing project funding. **Stephanie M. Willerth:** Project supervision, manuscript review and editing. **Haakon B. Nygaard:** Conceptualization, writing original draft, manuscript review and editing, project supervision and administration, project funding.

## Data availability

Data will be made available on request.

## Acknowledgements

This work was funded in part by the Weston Brain Institute, grant #TR150199 to HBN, and institutional funding to HBN and BAM.

## Appendix A. Supplementary data

Supplementary data to this article can be found online at <https://doi.org/10.1016/j.nbd.2023.106124>.

## References

- Baker, M., et al., 2006. Mutations in progranulin cause tau-negative frontotemporal dementia linked to chromosome 17. *Nature* 442 (7105), 916–919.
- Bardy, C., et al., 2015. Neuronal medium that supports basic synaptic functions and activity of human neurons in vitro. *Proc. Natl. Acad. Sci. U. S. A.* 112 (20), E2725–E2734.
- Bi, D., et al., 2020. GABAergic dysfunction in excitatory and inhibitory (E/I) imbalance drives the pathogenesis of Alzheimer's disease. *Alzheimers Dement.* 16 (9), 1312–1329.
- Bott, N.T., et al., 2014. Frontotemporal dementia: diagnosis, deficits and management. *Neurodegener. Dis. Manag.* 4 (6), 439–454.
- Chitramuthu, B.P., Campos-Garcia, V.R., Bateman, A., 2021. Multiple molecular pathways are influenced by Progranulin in a neuronal cell model—a parallel omics approach. *Front. Neurosci.* 15, 775391.
- Cruts, M., et al., 2006. Null mutations in progranulin cause ubiquitin-positive frontotemporal dementia linked to chromosome 17q21. *Nature* 442 (7105), 920–924.
- de Majo, M., et al., 2023. Granulin loss of function in human mature brain organoids implicates astrocytes in TDP-43 pathology. *Stem Cell Rep.* 18 (3), 706–719.
- Frew, J., Nygaard, H.B., 2021. Neuropathological and behavioral characterization of aged Grn R493X progranulin-deficient frontotemporal dementia knockin mice. *Acta Neuropathol. Commun.* 9 (1), 57.
- Frew, J., et al., 2020. Premature termination codon readthrough upregulates progranulin expression and improves lysosomal function in preclinical models of GRN deficiency. *Mol. Neurodegener.* 15 (1), 21.
- García-León, J.A., et al., 2018. Generation of a human induced pluripotent stem cell-based model for tauopathies combining three microtubule-associated protein TAU mutations which displays several phenotypes linked to neurodegeneration. *Alzheimers Dement.* 14 (10), 1261–1280.
- Götzl, J.K., et al., 2018. Early lysosomal maturation deficits in microglia triggers enhanced lysosomal activity in other brain cells of progranulin knockout mice. *Mol. Neurodegener.* 13 (1), 48.
- Hallmann, A.L., et al., 2017. Astrocyte pathology in a human neural stem cell model of frontotemporal dementia caused by mutant TAU protein. *Sci. Rep.* 7, 42991.
- Hedegaard, A., et al., 2020. Pro-maturational effects of human iPSC-derived cortical astrocytes upon iPSC-derived cortical neurons. *Stem Cell Rep.* 15 (1), 38–51.
- Henstridge, C.M., Tzioras, M., Paolicelli, R.C., 2019. Glial contribution to excitatory and inhibitory synapse loss in neurodegeneration. *Front. Cell. Neurosci.* 13, 63.
- Hogan, D.B., et al., 2016. The prevalence and incidence of frontotemporal dementia: a systematic review. *Can. J. Neurol. Sci.* 43 (Suppl. 1), S96–S109.
- Hong, S., et al., 2016. Complement and microglia mediate early synapse loss in Alzheimer mouse models. *Science* 352 (6286), 712–716.
- Lee, S.E., et al., 2019. Thalamo-cortical network hyperconnectivity in preclinical progranulin mutation carriers. *Neuroimage Clin.* 22, 101751.
- Lepeta, K., et al., 2016. Synaptopathies: synaptic dysfunction in neurological disorders - a review from students to students. *J. Neurochem.* 138 (6), 785–805.

- Lui, H., et al., 2016. Progranulin deficiency promotes circuit-specific synaptic pruning by microglia via complement activation. *Cell* 165 (4), 921–935.
- Mackenzie, I.R., 2007. The neuropathology and clinical phenotype of FTD with progranulin mutations. *Acta Neuropathol.* 114 (1), 49–54.
- Nicholson, A.M., et al., 2012. Progranulin axis and recent developments in frontotemporal lobar degeneration. *Alzheimers Res. Ther.* 4 (1), 4.
- Olszewska, D.A., et al., 2016. Genetics of frontotemporal dementia. *Curr. Neurol. Neurosci. Rep.* 16 (12), 107.
- Petkau, T.L., et al., 2010. Progranulin expression in the developing and adult murine brain. *J. Comp. Neurol.* 518 (19), 3931–3947.
- Petkau, T.L., et al., 2012. Synaptic dysfunction in progranulin-deficient mice. *Neurobiol. Dis.* 45 (2), 711–722.
- Rabinovici, G.D., Miller, B.L., 2010. Frontotemporal lobar degeneration: epidemiology, pathophysiology, diagnosis and management. *CNS Drugs* 24 (5), 375–398.
- Rose, S.E., et al., 2018. Leptomeninges-derived induced pluripotent stem cells and directly converted neurons from autopsy cases with varying Neuropathologic backgrounds. *J. Neuropathol. Exp. Neurol.* 77 (5), 353–360.
- Sretavan, D.W., Shatz, C.J., Stryker, M.P., 1988. Modification of retinal ganglion cell axon morphology by prenatal infusion of tetrodotoxin. *Nature* 336 (6198), 468–471.
- Suh, H.S., et al., 2012. Regulation of progranulin expression in human microglia and proteolysis of progranulin by matrix metalloproteinase-12 (MMP-12). *PLoS One* 7 (4), e35115.
- Tapia, L., et al., 2011. Progranulin deficiency decreases gross neural connectivity but enhances transmission at individual synapses. *J. Neurosci.* 31 (31), 11126–11132.
- Zhang, J., et al., 2020. Neurotoxic microglia promote TDP-43 proteinopathy in progranulin deficiency. *Nature* 588 (7838), 459–465.